

Polarized Balmer Line Emission from Supernova Remnant Shock Waves Efficiently Accelerating Cosmic Rays

Jiro Shimoda,^{1*} Yutaka Ohira,¹ Ryo Yamazaki,¹ J. Martin Laming²
and Satoru Katsuda³

¹*Department of Physics and Mathematics, Aoyama-Gakuin University, Sagamihara, Kanagawa 252-5258, Japan*

²*Space Science Division, Naval Research Laboratory, Code 7684, Washington DC 20375, USA*

³*Department of Physics, Faculty of Science & Engineering, Chuo University, 1-13-27 Kasuga, Bunkyo, Tokyo 112-8551, Japan*

Accepted XXX. Received YYY; in original form ZZZ

ABSTRACT

Linearly polarized Balmer line emissions from supernova remnant shocks are studied taking into account the energy loss of the shock owing to the production of nonthermal particles. The polarization degree depends on the downstream temperature and the velocity difference between upstream and downstream regions. The former is derived once the line width of the broad component of the H α emission is observed. Then, the observation of the polarization degree tells us the latter. At the same time, the estimated value of the velocity difference independently predicts adiabatic downstream temperature that is derived from Rankine-Hugoniot relations for adiabatic shocks. If the actually observed downstream temperature is lower than the adiabatic temperature, there is a missing thermal energy which is consumed for particle acceleration. It is shown that a larger energy loss rate leads to more highly polarized H α emission. Furthermore, we find that polarized intensity ratio of H β to H α also depends on the energy loss rate and that it is independent of uncertain quantities such as electron temperature, the effect of Lyman line trapping and our line of sight.

Key words: ISM:supernova remnants – cosmic rays – shock waves – atomic processes – polarization – acceleration of particles

1 INTRODUCTION

Supernova remnants (SNRs) are the best candidate sites for Galactic cosmic-ray (CR) production. Measurements of Galactic CR energy density around the Earth require that roughly a tenth of supernova explosion energy is consumed for CR acceleration. The CR acceleration efficiency at SNRs is estimated as an energy loss rate of the SNR shock wave (e.g. Hughes, Rakowski & Decourchelle 2000; Warren et al. 2005; Tatischeff & Hernanz 2007; Helder et al. 2009, 2013; Morlino et al. 2013a, 2014). Since the shock loses its kinetic energy due to the CR acceleration, the downstream temperature becomes lower than that in the adiabatic case. Therefore, if we measure both the downstream temperature (T_{down}) and the shock velocity (V_{sh}) independently, we can estimate the energy loss rate. In order to do this, we define $kT_{\text{RH}} = \frac{3}{16}\mu m_{\text{p}}V_{\text{sh}}^2$ (k is Boltzmann constant and μ is the mean molecular weight), which is the adiabatic downstream temperature predicted by Rankine-Hugoniot relations in the strong shock limit without CR acceleration (that is, the

adiabatic shocks). Then, the energy loss rate is defined as Shimoda et al. (2015)

$$\eta = \frac{T_{\text{RH}} - T_{\text{down}}}{T_{\text{RH}}}. \quad (1)$$

Observations of SNR RCW 86 give an example. The shock velocity is measured by the proper motion of an H α filament as $V_{\text{sh}} \approx 1800$ km/s, that gives $T_{\text{RH}} \approx 4 \text{ keV}(\mu/0.62)(V_{\text{sh}}/1800 \text{ km s}^{-1})^2$ (Helder et al. 2013). On the other hand, the downstream temperature is derived from spectroscopy of the H α emission as $T_{\text{down}} \approx 2 \text{ keV}$ (Helder et al. 2009). Combining these observations, we obtain $\eta \approx 0.5$.¹ Such extremely high energy loss rate would alter the long-term evolution of the shock (e.g. Cohen, Piran & Sari 1998; Liang & Keilby 2000). However,

¹ In Helder et al. (2013), the proper motions of H α filaments were observed as 1871 ± 250 , 1196 ± 367 and $1325 \pm 221 \text{ km s}^{-1}$ at the region where the downstream temperature was measured. The adiabatic downstream temperatures are calculated as $kT_{\text{RH}} = 4.5 \pm 1.2$, 1.8 ± 1.1 and $2.3 \pm 0.7 \text{ keV}$, respectively, resulting in $\eta = 0.6 \pm 0.1$, -0.08 ± 0.7 and 0.1 ± 0.3 , respectively.

* E-mail: s-jiro@phys.aoyama.ac.jp (JS)

to evaluate the shock velocity from the proper motion measurements, we need a distance to the SNR with high accuracy, which is often hard in astronomy. In this paper, following work by [Laming \(1990\)](#), we show that the energy loss rate can be obtained by polarization degree of the H α emissions without precise measurements of the distance.

We will briefly review the H α emissions in SNRs. The young SNR shock is formed by the interaction between charged particles and plasma waves rather than particle Coulomb collision processes (so called collisionless shock). The shock wave propagates into the interstellar medium (ISM), which is in general partially ionized. The charged particles in ISM are heated by the collisionless shock wave, while the neutral particles (hereafter, we consider only hydrogen atoms) are not affected. Therefore, the hydrogen atoms collide with charged particles in the downstream region owing to a finite relative velocity. As a result, the hydrogen atoms entering the downstream region are excited, radiating Balmer line emissions, and they are eventually ionized. Since the length of the emitting region, which is on the order of the mean free path of atomic collision, $\sim 10^{16}$ cm, is much shorter than the radius of SNR (~ 1 -10 pc), the Balmer line emissions are bright along the shock surface on the sky. Such SNR shocks are called as Balmer dominated shocks (BDSs, e.g. [Chevalier & Raymond 1978](#); [Chevalier, Kirshner & Raymond 1980](#); [Laming 1990](#); [Heng & McCray 2007](#); [Heng 2010](#); [van Adelsberg et al. 2008](#); [Morlino et al. 2012](#)). In addition, the H α emissions from the upstream region have been observed in some SNRs (e.g. [Ghavamian et al. 2000](#); [Lee et al. 2007, 2010](#); [Katsuda et al. 2016](#)). The spectrum of the Balmer line emissions often consists of narrow and broad components. The former is caused by the direct excitation via collision between the hydrogen atoms and the charged particles. On the other hand, the latter is emitted after the charge exchange reaction between the hydrogen atoms entering the shock and the downstream heated protons. Hence, the width of the narrow component reflects thermal/nonthermal velocity of upstream hydrogen atoms (often observed as ~ 20 -50 km s $^{-1}$: [Medina et al. 2014](#); [Knežević et al. 2016](#)), and the width of the broad component reflects the downstream proton temperature (e.g. ~ 2000 km s $^{-1}$: [Chevalier, Kirshner & Raymond 1980](#)). Thus, the downstream proton temperature can be directly measured from the width of broad H α emission ([Chevalier, Kirshner & Raymond 1980](#)). It is also possible to measure the electron temperature, the heating process of electrons in the formation of collisionless shock is a matter of debate and still widely studied (e.g. [Cargill & Papadopoulos 1988](#); [Ghavamian et al. 2001, 2002](#); [Ohira & Takahara 2007, 2008](#); [Rakowski, Laming & Ghavamian 2008](#)). In BDS, the intensity ratio of the broad to the narrow component depends on temperature equilibration between ions and electrons (e.g. [van Adelsberg et al. 2008](#)). Therefore, the electron temperature is derived by the intensity ratio of the broad to the narrow component (e.g. [Ghavamian et al. 2001, 2002](#); [van Adelsberg et al. 2008](#); [Morlino et al. 2012, 2013b](#)). BDS is seen in a number of SNRs. Moreover, measurements of the Balmer line nature could be an essential probe of the collisionless shock physics.

Some of the hot hydrogen atoms emerging from the charge-exchange reaction can leak upstream because they

do not feel electromagnetic fields. The leaking hot hydrogen atoms are ionized again through the collision with incoming charged particles. As a result, the hot protons are injected in the upstream region ([Lim & Raga 1996](#); [Blasi et al. 2012](#); [Ohira 2012](#)). The injected protons can be scattered by electromagnetic waves in the region adjacent to the shock and accelerated by diffusive shock acceleration (e.g. [Ohira 2012, 2013, 2016a,b](#)). Therefore, BDSs are expected to be an accelerator of CR protons.

Recently, [Sparks et al. \(2015\)](#) discovered linearly polarized H α emission with 2.0 ± 0.4 per cent polarization degree in the north-west region of the young SNR, SN 1006, in good agreement with the original prediction of [Laming \(1990\)](#). In laboratory experiments, linearly polarized H α emission from hydrogen atoms in electron beams has been measured with ~ 40 per cent polarization degree (e.g. [Kleinpoppen & Kraiss 1968](#)). The measurements of polarized atomic lines act as strong tools to study atomic structure. The electron beam, which collides with hydrogen atoms from only one direction, behaves as a quantization axis of the orbital angular momentum of bound electron in excited hydrogen atoms (e.g. [Takács et al. 1996](#)). The collisional excitation is essentially nonrelativistic and can be discussed in terms of orbital angular momenta. Once excited the orbital angular momentum of the electron couples to its spin angular momentum to form a total angular momentum, j , with z -component m_j . The bound electrons lose their energy and total angular momentum owing to the spontaneous transition, and emit photons. The polarization of the photon is then determined to be linear or circular by a variation of the orbital angular-momentum component along with the beam direction, which is given by magnetic quantum number m_j . The linearly polarized intensity becomes largest when viewed from the direction orthogonal to the beam. For BDS, charged hot particles hit cold hydrogen atoms from various directions in the downstream region. In the rest frame of hydrogen atoms (i.e. the upstream frame), the colliding charged particles are seen as a mildly-collimated beam. Therefore, this anisotropy eventually causes the net polarization of the line emission, with the polarization degree of a few percent.

If the SNR shock with shock velocity V_{sh} efficiently accelerates CRs, then they can escape the shock, carrying away significant energy. As a result, the downstream temperature becomes lower than T_{RH} , yielding larger anisotropy of the particle velocity downstream. [Laming \(1990\)](#) studied the linearly polarized H α emission from BDS without CR acceleration. Then, he showed that a few-10 per cent polarization degree can be observed. His study was limited owing to the lack of atomic data on proton collisional excitation cross section and the line of sight direction was fixed as orthogonal to the shock normal, which gives the largest linear polarization degree. [Heng & Sunyaev \(2008\)](#) and [Tselikhovich, Hirata & Heng \(2012\)](#) updated the atomic data and fitting functions. Using their data, we study the linearly polarized Balmer line emissions from the SNR shocks losing their thermal energy. We show that a higher energy loss rate causes higher polarization degree. The polarization degree of the line emission is determined by the anisotropy of the velocity distribution of charged particles (i.e. collimation of incident beam), which is given by the downstream temperature and the upstream fluid velocity. We can measure the downstream temperature from

the width of the broad H α line, whereas the downstream fluid velocity is derived from the polarization measurements. Since the shock velocity V_{sh} relates T_{RH} by Rankine-Hugoniot relation, we can obtain the energy loss rate η without measuring of SNR distance. In Sect. 2, we formulate the polarized Balmer line emissions from the shock accelerating nonthermal particles. In Sect. 3, we present the results of polarization degree of H α . In Sect. 4, the polarized intensity ratio of H β to H α is discussed. Finally, we summarize our results and discuss on future prospects for the estimation of η .

2 PHYSICAL MODEL

In Laming (1990), only the case of viewing angle orthogonal to the shock normal was considered. In this paper, we extend his study, and investigate the linearly polarized Balmer-emission from the shock, which loses kinetic energy due to CR acceleration, with arbitrary viewing angle. In the following, we consider only the narrow component of H α and H β emissions resulting from the direct collisional excitation and denoting by “n”.

2.1 The Model Geometry

Figure 1 shows the schematic diagram of the shock geometry. The blue sheet is $z = 0$ plane and represents the shock surface. The blue arrow shows the downstream velocity in the upstream rest frame, which is parallel to the z axis. The purple vector is the velocity of the particle q that collides with the hydrogen atom at the origin,

$$\mathbf{v}_q = (v_q \sin \theta \cos \varphi, v_q \sin \theta \sin \varphi, v_q \cos \theta).$$

The red y' axis is parallel to the line of sight and the red z' axis is perpendicular, which makes an angle χ to the y axis. The red sheet represents the plane of the sky, which is orthogonal to the line of sight.

2.2 The Polarized Line Emission

Polarized atomic line emission induced by collisional excitation is reviewed by Percival & Seaton (1958). In this paper, we treat the dipole transition that makes Balmer line emission.

Let $\sigma_{nlm_l, q}$ be the cross section of collisional excitation by the particle q from the ground state hydrogen atom to the excited state nlm_l , where n is the principal quantum number, $l = 0, 1, \dots, n-1$ is the orbital angular momentum quantum number and $m_l = -l, -l+1, \dots, l$ is the magnetic quantum number. We evaluate the orbital angular momentum of the bound electron of the hydrogen atom along the incident direction of the particle q . Then, the quantum number l represents the orbital angular momentum magnitude of the bound electron, $L = \sqrt{l(l+1)}\hbar$, while the magnetic quantum number m_l gives the component of the orbital angular momentum parallel to \mathbf{v}_q , $L_r = m_l \hbar$. Let $A_{njm_j, n'j'm'_j}$ be the spontaneous transition rate per unit time from the atomic state of nlm_l to $n'j'm'_j$. The total angular momentum j is formed by vector addition of l and s , the orbital and spin angular momenta, and this coupling introduces some depolarization. The spontaneous transition is only allowed for

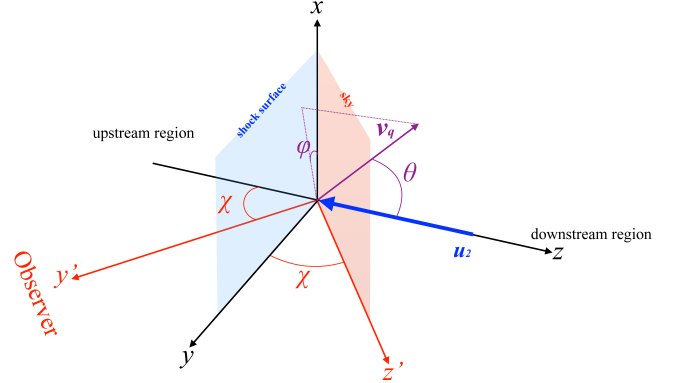


Figure 1. Schematic diagram of the shock geometry. The blue x - y plane ($z = 0$) represents the shock surface. The blue arrow \mathbf{u}_z shows the downstream velocity in the upstream rest frame, which is parallel to the z axis. The purple vector \mathbf{v}_q is the velocity of the particle q , that collides with the hydrogen atom at the origin. The red y' axis is parallel to the line of sight and the red z' axis is orthogonal to x - y' plane, and makes an angle χ with the z axis. The red x - z' plane represents the plane of the sky, which is orthogonal to the line of sight.

$\Delta l = l - l' = \pm 1$ and $|\Delta m_l| = |m - m'| \leq 1$, $\Delta j \leq 1$ and $|\Delta m_j| \leq 1$. In what follows however, we adopt a nonrelativistic description of the hydrogen atom for decay rates and branching ratios, i.e. using $A_{nlm_l, n'l'm'_l}$ instead of $A_{njm_j, n'j'm'_j}$, and we drop the l or j subscript on Δm .

By the conservation of the angular momentum, the polarization of emitted photon is characterized by the subtraction of the eigenvalues of L_r before and after the transition. We presume that the transition of the hydrogen atom induces second time derivative of electric dipole moment whose polarization vector is $\hat{d}_{\Delta m}$. The polarization vector can be written as

$$\begin{aligned} \hat{d}_0 &= \hat{v}_{q,r} e^{i\omega_B t}, \\ \hat{d}_{\pm 1} &= \frac{1}{\sqrt{2}} (\hat{v}_{q,\theta} \pm i \hat{v}_{q,\varphi}) e^{i\omega_B t}, \end{aligned} \quad (2)$$

where unit vectors are defined as

$$\begin{aligned} \hat{v}_{q,r} &= (\sin \theta \cos \varphi, \sin \theta \sin \varphi, \cos \theta), \\ \hat{v}_{q,\theta} &= (\cos \theta \cos \varphi, \cos \theta \sin \varphi, -\sin \theta), \\ \hat{v}_{q,\varphi} &= \hat{v}_{q,r} \times \hat{v}_{q,\theta} = (-\sin \varphi, \cos \varphi, 0), \end{aligned}$$

and i is imaginary unit, and ω_B is the angular frequency of the Balmer-series emission. The electric field of the photon emitted along the line of sight direction is given by

$$\mathbf{E}_{\Delta m}(t) = \left\{ \hat{y}' \times (\hat{y}' \times \hat{d}_{\Delta m}) \right\} E(t), \quad (3)$$

where the unit vector along the line of sight is

$$\hat{y}' = (0, \sin \chi, -\cos \chi),$$

and $E(t)$ is the electric field strength. We decompose the observed electric field as

$$\begin{aligned} \mathbf{E}_{\Delta m, z'} &= (\mathbf{E}_{\Delta m} \cdot \hat{z}') \hat{z}', \\ \mathbf{E}_{\Delta m, x} &= (\mathbf{E}_{\Delta m} \cdot \hat{x}) \hat{x}, \end{aligned}$$

where the basic vectors are written as

$$\begin{aligned} \hat{z}' &= (0, \cos \chi, \sin \chi), \\ \hat{x} &= (1, 0, 0). \end{aligned}$$

The observed intensity of the line emission is proportional to the number of hydrogen atoms that yield $\hat{d}_{\Delta m}$. Let $\sigma'_{\Delta m, q}$ be the cross section inducing $\hat{d}_{\Delta m}$ resulting from the collision between the particle q and the hydrogen atom as

$$\begin{aligned} \sigma'_{\Delta m, q}(v_q) &= \sum_{\substack{l'=l\pm 1 \\ m'_l=m_l+\Delta m}} B_{nlm_l, n'l'm'_l} \sigma_{nlm_l, q}(v_q), \\ B_{nlm_l, n'l'm'_l} &= \frac{A_{nlm_l, n'l'm'_l}}{\sum_{n', l', m'_l} A_{nlm_l, n'l'm'_l}}, \end{aligned} \quad (4)$$

where $B_{nlm_l, n'l'm'_l}$ is the branching ratio of the spontaneous transition from the atomic level nlm_l to $n'l'm'_l$. For fixed n and n' , we take the summation of $\sigma_{\Delta m, q}$ for l, l', m, m' under the constraints $l - l' = \pm 1$, $\Delta m = 0$ or ± 1 . In the following, we regard $\sigma'_{1, q}$ as identical to $\sigma'_{-1, q}$ because the collision between the particle q and the hydrogen atom is axially symmetric. The Stokes parameters of the observed line emission are written as

$$\begin{aligned} Q_n &= \langle E_{\text{obs}, z'} E_{\text{obs}, z'}^* \rangle - \langle E_{\text{obs}, x} E_{\text{obs}, x}^* \rangle, \\ I_n &= \langle E_{\text{obs}, z'} E_{\text{obs}, z'}^* \rangle + \langle E_{\text{obs}, x} E_{\text{obs}, x}^* \rangle, \end{aligned}$$

where $E_{\text{obs}, z'}$ ($E_{\text{obs}, x}$) is z' (x) components of the observed electric field, the asterisk $*$ represents the complex conjugate, and $\langle EE^* \rangle = \int_0^T EE^* / T dt$ means long-time average in the random phase approximation. Let $f_q(\mathbf{v}_q, \mathbf{u}_2)$ be a velocity distribution function of particle q . We approximate the velocity distribution function of hydrogen atom as Dirac delta function, $\delta(\mathbf{v}_\mathbf{H})$. Then, the observed Stokes parameters are

$$\begin{aligned} Q_n &= n_{\text{H}} \sum_q n_q \int v_q f_q(\mathbf{v}_q, \mathbf{u}_2) \\ &\times \left[\sigma'_{0, q} |\mathbf{E}_{0, z'}|^2 + \sigma'_{1, q} |\mathbf{E}_{1, z'}|^2 + \sigma'_{-1, q} |\mathbf{E}_{-1, z'}|^2 \right. \\ &\left. - \left\{ \sigma'_{0, q} |\mathbf{E}_{0, x}|^2 + \sigma'_{1, q} |\mathbf{E}_{1, x}|^2 + \sigma'_{-1, q} |\mathbf{E}_{-1, x}|^2 \right\} \right] d^3 \mathbf{v}_q \\ &= n_{\text{H}} E^2 \sum_q n_q \int v_q f_q(\mathbf{v}_q, \mathbf{u}_2) \\ &\times \left[\sigma'_{0, q} |\hat{z}' \cdot \hat{\mathbf{v}}_{q, r}|^2 + \sigma'_{1, q} \left(|\hat{z}' \cdot \hat{\mathbf{v}}_{q, \theta}|^2 + |\hat{z}' \cdot \hat{\mathbf{v}}_{q, \varphi}|^2 \right) \right. \\ &\left. - \left\{ \sigma'_{0, q} |\hat{x} \cdot \hat{\mathbf{v}}_{q, r}|^2 + \sigma'_{1, q} \left(|\hat{x} \cdot \hat{\mathbf{v}}_{q, \theta}|^2 + |\hat{x} \cdot \hat{\mathbf{v}}_{q, \varphi}|^2 \right) \right\} \right] d^3 \mathbf{v}_q, \end{aligned} \quad (5)$$

and likewise

$$\begin{aligned} I_n &= n_{\text{H}} E^2 \sum_q n_q \int v_q f_q(\mathbf{v}_q, \mathbf{u}_2) \\ &\times \left[\sigma'_{0, q} |\hat{z}' \cdot \hat{\mathbf{v}}_{q, r}|^2 + \sigma'_{1, q} \left(|\hat{z}' \cdot \hat{\mathbf{v}}_{q, \theta}|^2 + |\hat{z}' \cdot \hat{\mathbf{v}}_{q, \varphi}|^2 \right) \right. \\ &\left. + \left\{ \sigma'_{0, q} |\hat{x} \cdot \hat{\mathbf{v}}_{q, r}|^2 + \sigma'_{1, q} \left(|\hat{x} \cdot \hat{\mathbf{v}}_{q, \theta}|^2 + |\hat{x} \cdot \hat{\mathbf{v}}_{q, \varphi}|^2 \right) \right\} \right] d^3 \mathbf{v}_q, \end{aligned} \quad (6)$$

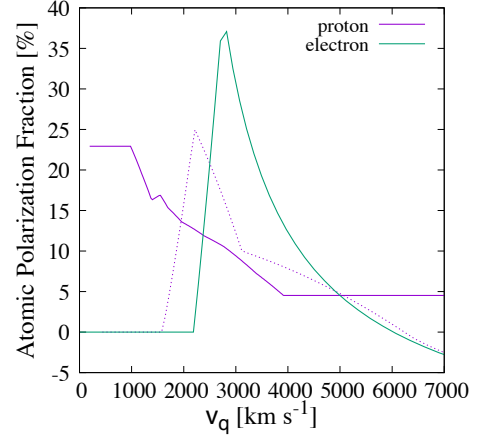


Figure 2. The atomic polarization fraction as a function of the colliding particle velocity v_q for the proton (magenta line) and electron impacts (green line). The dotted line was assumed in Laming (1990) for proton impact.

where n_{H} and n_q are the number density of the hydrogen atom and particle q . In the following, we consider only protons (denoted as “p”) and electrons (denoted as “e”) as the particle q which excite the hydrogen atoms (i.e. $q = \{\text{p}, \text{e}\}$ and $n_p = n_e$). When the ionization degree of the upstream medium is significantly low, the collisional excitation by hot hydrogen atoms emerged from the charge-exchange reaction would also contribute to the production of Balmer photons. Indeed, the cross section of the collisional excitation on the impact between proton and hydrogen atom is comparable with that between two hydrogen atoms (e.g. Barnett et al. 1990). We neglect this process for simplicity.

2.3 Cross Sections of Impact Excitation

In order to calculate the Stokes parameters from Eqs. (5) and (6), the data for the cross section, $\sigma'_{\Delta m_l, q}$, are required. In the laboratory experiment, the values of $\sigma'_{\Delta m_l, q}$ are derived by measuring the polarization degree of Balmer emissions resulting from the collision between hydrogen atoms and a charged particle beam (e.g. McConkey 1988).

If we set $\chi = \pi/2$ and $f_q = \delta(\mathbf{v}_q - \mathbf{u}_2)$ with $\mathbf{u}_2 = (0, 0, u_2)$ in the Eqs. (5) and (6), then the observed polarization degree is derived as

$$\frac{Q_n}{I_n} = \sum_q \frac{\sigma'_{0, q} - \sigma'_{1, q}}{\sigma'_{0, q} + \sigma'_{1, q}}.$$

Thus, the polarization degree, P_q , of the line emission radiated from the hydrogen atom in the direction perpendicular to the incident direction of particle q is written as

$$P_q = \frac{\sigma'_{0, q} - \sigma'_{1, q}}{\sigma'_{0, q} + \sigma'_{1, q}}, \quad (7)$$

which is called the atomic polarization fraction. In the following, we use the notations (s, p, d, f, ...) = (0, 1, 2, 3, ...) as the orbital angular momentum quantum number, l , which are often used in atomic spectroscopy and astronomy.

Table 1. The branching ratio of H α and H β (e.g. Heng & Sunyaev 2008).

$B_{3p,2s}$	0.1183
$B_{4s,2p}$	0.5841
$B_{4s,3p}$	0.4159
$B_{4p,1s}$	0.8402
$B_{4p,2s}$	0.1191
$B_{4p,3s}$	3.643×10^{-2}
$B_{4p,3d}$	4.282×10^{-3}
$B_{4d,2p}$	0.7456
$B_{4d,3p}$	0.2544

Percival & Seaton (1958) and Syms et al. (1975) theoretically gave the fraction of H α as

$$P_q(\text{H}\alpha) = \left[B_{3p,2s} \frac{\sigma_{3p0,q} - \sigma_{3p\pm 1,q}}{2} + 57 \frac{\sigma_{3d0,q} + \sigma_{3d\pm 1,q} - 2\sigma_{3d\pm 2,q}}{100} \right] \times \left[\sigma_{3s0,q} + B_{3p,2s} \frac{7\sigma_{3p0,q} + 11\sigma_{3p\pm 1,q}}{6} + \frac{119\sigma_{3d0,q} + 219\sigma_{3d\pm 1,q} + 162\sigma_{3d\pm 2,q}}{100} \right]^{-1}, \quad (8)$$

where $\sigma_{nl\pm m,q} = \sigma_{nl+m,q} + \sigma_{nl-m,q}$. The numerical coefficients are considering the spin-orbit interaction, but neglecting hyperfine structure. For the proton impact in the range of $1000 \text{ km s}^{-1} \lesssim v_p \lesssim 4000 \text{ km s}^{-1}$, we can use the data derived by Tselikhovich, Hirata & Heng (2012). Balança & Feautrier (1998) showed that the atomic polarization fraction of H α is almost constant (≈ 0.25) for $v_p \lesssim 1000 \text{ km s}^{-1}$. Thus, we assume $P_p(\text{H}\alpha)|_{v_p \leq 1000 \text{ km s}^{-1}} = P_p(\text{H}\alpha)|_{v_p = 1000 \text{ km s}^{-1}}$ and $P_p(\text{H}\alpha)|_{v_p \geq 4000 \text{ km s}^{-1}} = P_p(\text{H}\alpha)|_{v_p = 4000 \text{ km s}^{-1}}$. For the fraction from electron impact, we follow the approximation by Laming (1990) given as

$$P_e(\text{H}\alpha) = \begin{cases} 0 & \text{for } E_e < 0.5, \\ \frac{4-3 \ln E_e}{14.3+11 \ln E_e} & \text{for } 0.794 \leq E_e, \\ 1.36(E_e - 0.5) & \text{for } 0.5 \leq E_e \leq 0.794, \end{cases} \quad (9)$$

where E_e is the collision energy of the electron in the rest frame of hydrogen atom (in atomic units). The atomic polarization fraction of H β is hardly studied, compared with H α and Ly α . On the other hand, the fraction of Ly β is almost the same as Ly α (Balança & Feautrier 1998). In the following, we assume the polarization fraction of H β is the same as that of H α . Figure 2 shows the atomic polarization fraction following proton (magenta line) and the electron impacts (green line). The dotted line represents the fraction for the proton impact assumed in Laming (1990). With the updated data of the atomic polarization fraction, we obtain smaller polarization degree compared with the previous work by Laming (1990) at high proton temperatures, and larger polarization at low proton temperature where he assumed the polarization to be zero. Since the total cross section yielding the line emission on particle q impact is $\sigma_{\text{tot},q} = \sigma'_{0,q} + 2\sigma'_{1,q}$, we can derive (Laming 1990)

$$\sigma'_{0,q} + \sigma'_{1,q} = \frac{2}{3 - P_q} \sigma_{\text{tot},q}, \quad (10)$$

$$\sigma'_{0,q} - \sigma'_{1,q} = P_q(\sigma'_{0,q} + \sigma'_{1,q}). \quad (11)$$

The total cross section $\sigma_{\text{tot},q}$ is the summation of

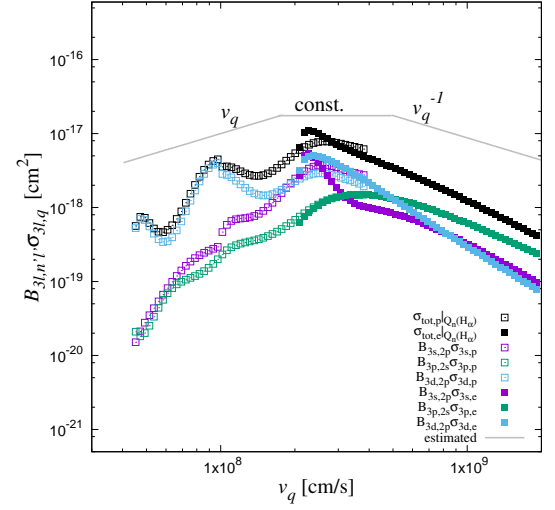


Figure 3. The cross section of direct excitation to $n = 3$ level for proton impact (open squares) and electron impact (closed squares), $B_{3l,n'l'} \sigma_{3l,q}$. The black squares are $\sigma_{\text{tot},q} |_{Q_n(\text{H}\alpha)}$.

$B_{nl,n'l'} \sigma_{nl,q}^*$, where $B_{nl,n'l'}$ is the branching ratio of the spontaneous transition from the atomic state nl to $n'l'$, which is summarized in Table 1. The $\sigma_{nl,q}^*$ is the effective cross section for particle q impact on the ground state hydrogen including the effect of cascading from higher atomic levels. Here, we omit the magnetic quantum number m because it does not contribute the total cross section and the branching ratio. The total cross sections inducing the H α emission are written as

$$\sigma_{\text{tot},q} |_{Q_n(\text{H}\alpha)} = \sigma_{3s,q} + B_{3p,2s} \sigma_{3p,q} + \sigma_{3d,q}, \quad (12)$$

$$\sigma_{\text{tot},q} |_{I_n(\text{H}\alpha)} = \sigma_{3s,q}^* + B_{3p,2s} \sigma_{3p,q}^* + \sigma_{3d,q}^*, \quad (13)$$

$$\sigma_{3s,q}^* = \sigma_{3s,q} + B_{4p,3s} \sigma_{4p,q}, \quad (14)$$

$$\sigma_{3p,q}^* = \sigma_{3p,q} + B_{4s,3p} \sigma_{4s,q} + B_{4d,3p} \sigma_{4d,q}, \quad (15)$$

$$\sigma_{3d,q}^* = \sigma_{3d,q} + B_{4p,3d} \sigma_{4p,q} + \sigma_{4f,q}, \quad (16)$$

where we assume the emission resulting from the cascade from the level with $n > 3$ is unpolarized. The cascade affects the observed polarization by a factor of ~ 5 per cent (Laming 1990). Neglecting the cascades from higher atomic levels, we give the total cross sections inducing the H β emissions as

$$\sigma_{\text{tot},q} |_{I_n, Q_n(\text{H}\beta)} = B_{4s,2p} \sigma_{4s,q} + B_{4p,2s} \sigma_{4p,q} + B_{4d,2p} \sigma_{4d,q}. \quad (17)$$

Figures 3 and 4 represent $B_{nl,n'l'} \sigma_{nl,q}$ for H α and H β emissions, respectively. Here we take data from Janev & Smith (1993), Bray & Stelb (1995), Heng & Sunyaev (2008) and Tselikhovich, Hirata & Heng (2012). For $v_p \lesssim 1000 \text{ km s}^{-1}$, we use the data given by Balança & Feautrier (1998), which were calculated with the close-coupling approximation. This approximation is known to be applicable for the range of $v_p \ll \alpha c$ (e.g. Tselikhovich, Hirata & Heng 2012), where $\alpha = 1/137$ is the fine structure constant. In particular, the proton cross section data in the range $1000 \text{ km s}^{-1} \lesssim v_p \lesssim 4000 \text{ km s}^{-1}$

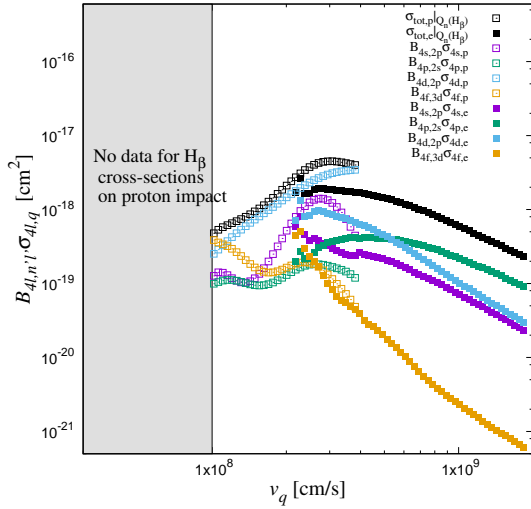


Figure 4. The cross section for direct excitation to $n = 4$ level by proton impact (open squares) and electron impact (closed squares), $B_{4l,n'l'}\sigma_{4l,q}$. The black squares are $\sigma_{\text{tot},q}|_{Q_n(\text{H}\beta)}$.

were derived by the direct numerical simulations by Tseliakhovich, Hirata & Heng (2012). Besides, we assume that the cross section for proton impact excitation in the range $v_p \gtrsim 4000 \text{ km s}^{-1}$ is the same as that of the electron impact excitation. Indeed, the proton impact cross section for $n = 3$ approaches to the electron’s one for $v_q \gtrsim 3000 \text{ km s}^{-1}$ (e.g. Janev & Smith 1993). The fitting functions of these data are provided by Heng & Sunyaev (2008) and Tseliakhovich, Hirata & Heng (2012). The data for $n = 4$ are unavailable for the range $v_p \lesssim 1000 \text{ km s}^{-1}$. We treat the cross section for proton impact to be zero in this range. The data for electron impact and their fitting functions are provided by International Atomic Energy Agency (<https://www-amdis.iaea.org/ALADDIN/>).

The time scale of the spontaneous transition of the hydrogen atom from the excited state to the ground state, $\sim 10^{-8}\text{-}10^{-1} \text{ s}$, is usually much shorter than the mean collision time of particle q , $\sim 10^8 \text{ s} \left(\frac{n_q}{1 \text{ cm}^{-3}}\right)^{-1} \left(\frac{\sigma}{10^{16} \text{ cm}^2}\right)^{-1} \left(\frac{v_q}{10^8 \text{ cm s}^{-1}}\right)^{-1}$ for SNR shocks. Therefore, we assume that all the hydrogen atoms are excited from the ground state (e.g. van Adelsberg et al. 2008).

2.4 Lyman Line Trapping

A part of hydrogen atoms in the states $n > 2$ emit Lyman-series photons (e.g. $3p \rightarrow 1s$). If the system is optically thick for the Lyman photon, the emitted Lyman photons are absorbed by the ground-state hydrogen atoms and eventually converted to other series as Balmer, Paschen and so on (e.g. Heng 2010). In such a situation, for instance, the branching ratio in Eq. (13) is effectively $B_{3p,2s} \approx 1$ (e.g. van Adelsberg et al. 2008). It is called ‘‘Case B’’. On the other hand, for optically thin limit (known as ‘‘Case A’’),

we can use the values of the branching ratio summarized in Table 1.

In this paper, we assume that the Balmer photons emitted by the absorption of Lyman photons are unpolarized. Therefore, for Case B, the branching ratios concerning I are approximately

$$\begin{aligned} B_{3p,2s} &= 1, \\ B_{4p,2s} &= 1 - B_{4p,3s} - B_{4p,3d}, \\ B_{4p,3s} &= 1 - B_{4p,2s} - B_{4p,3d}. \end{aligned}$$

2.5 Polarization from the Shock Wave

Using the atomic data given in previous sections, we calculate the Stokes parameters for an arbitrary velocity distribution of the particle q , $f_q(\mathbf{v}_q, \mathbf{u}_2)$. The velocity distribution function of particle q is set to a Maxwellian as

$$f_q(\mathbf{v}_q, \mathbf{u}_2) = \left(\frac{m_q}{2\pi kT_q}\right)^{\frac{3}{2}} \exp\left(-\frac{m_q(\mathbf{v}_q - \mathbf{u}_2)^2}{2kT_q}\right), \quad (18)$$

where m_q and k are respectively the mass of particle q and Boltzmann constant, T_q is the downstream temperature of particle q . Substituting Eq. (18) into Eqs. (5)-(6), and integrating $0 \leq \theta \leq \pi$ and $0 \leq \varphi \leq 2\pi$, we derive

$$\begin{aligned} Q_n &= 4\pi n_{\text{H}} E^2 \sin^2 \chi \sum_{q=e,p} n_q \left(\frac{D_q}{\pi}\right)^{\frac{3}{2}} \frac{e^{-D_q u_2^2}}{(2D_q u_2)^4} \\ &\times \int_0^\infty \alpha_q^3 e^{-\left(\frac{D_q \alpha_q}{2u_2}\right)^2} (\sigma_{0,q} - \sigma_{1,q}) \\ &\times \left[\left(\frac{3}{\alpha_q^3} + \frac{1}{\alpha_q} \right) \sinh \alpha_q - \frac{3}{\alpha_q^3} \cosh \alpha_q \right] d\alpha_q, \end{aligned} \quad (19)$$

and

$$\begin{aligned} I_n &= 4\pi n_{\text{H}} E^2 \sum_{q=e,p} n_q \left(\frac{D_q}{\pi}\right)^{\frac{3}{2}} \frac{e^{-D_q u_2^2}}{(2D_q u_2)^4} \int_0^\infty \alpha_q^3 e^{-\left(\frac{D_q \alpha_q}{2u_2}\right)^2} \\ &\times \left[(\sigma_{0,q} + \sigma_{1,q}) \frac{\sinh \alpha_q}{\alpha_q} \right. \\ &+ (\sigma_{0,q} - \sigma_{1,q}) \times \left. \left[\left(\frac{1 - 3 \cos^2 \chi}{\alpha_q^3} - \frac{\cos^2 \chi}{\alpha_q^2} \right) \sinh \alpha_q \right. \right. \\ &\left. \left. - \frac{1 - 3 \cos^2 \chi}{\alpha_q^2} \cosh \alpha_q \right] \right] d\alpha_q, \end{aligned} \quad (20)$$

where

$$\begin{aligned} D_q &= \frac{m_q}{2kT_q}, \\ \alpha_q &= 2D_q u_2 v_q, \\ u_2 &= |\mathbf{u}_2|. \end{aligned}$$

When $\chi = \pi/2$, Eqs. (19) and (20) coincide with Eqs. (8) and (9) of Laming (1990). In particular, when $\chi = \pi/2$ and $D_q u_2^2 = 0$, we obtain $Q_n = 0$ and $I_n \propto \int_0^\infty (\sigma_{0,q} + 2\sigma_{1,q}) e^{-D_q v_q^2} v_q^3 dv_q$, that is, the observed emission is unpolarized due to the almost isotropic collisions. On the other hand, when $D_q u_2^2 \rightarrow \infty$ leading to extremely anisotropic collisions, the observed emission is polarized as $Q_n/I_n = \sum(\sigma_{0,q} - \sigma_{1,q})/(\sigma_{0,q} + \sigma_{1,q})$.

When we observe the shock from right in front (i.e. $\chi = 0$), the observed emission is unpolarized due to the isotropic collisions between the particle q and the hydrogen atom.

2.6 Shock Jump Conditions

To calculate the polarization degree from Eqs. (19) and (20), we consider the downstream temperature T_q and the downstream velocity u_2 measured in the upstream rest frame. Since the kinetic energy of the shock is consumed for the acceleration of nonthermal particles, the downstream temperature becomes lower than that in the adiabatic case, T_{RH} . If all the accelerated particles escape from the system, the shock dynamics can be described like a radiative shock for optically thin limit.

Cohen, Piran & Sari (1998) analyzed the self-similar solution of the radiative shock. Their analysis is independent of the details of the cooling process. They considered that the cooling timescale is much shorter than the hydrodynamical timescale and the shocked medium radiates a fixed fraction of its internal energy in the cooling layer. In this case, the shock velocity is constant during the time that a given fluid element crosses the radiative zone and cools. Hence, the shock and the cooling layer are stationary. They additionally assumed that the radiation does not affect the shock structure, which remains adiabatic, and that the radiative layer follows it. In this paper, we follow Cohen, Piran & Sari (1998) to derive the shock jump conditions, and assume that all the hydrogen atoms collide with the charged particles behind the end of the cooling layer.

Assuming a polytropic equation of state with an adiabatic index γ , and a sufficiently high Mach number of the upstream flow, we obtain the downstream mass density ρ_1 , velocity measured in the shock frame u'_1 and pressure p_1 in the region immediately behind the shock front as

$$\begin{aligned} \rho_1 &= \frac{\gamma+1}{\gamma-1}\rho_0, \\ u'_1 &= \frac{\gamma-1}{\gamma+1}V_{sh}, \\ p_1 &= \frac{2}{\gamma+1}\rho_0V_{sh}^2, \end{aligned} \quad (21)$$

where ρ_0 and V_{sh} are the mass density of the upstream medium and the shock velocity, respectively. Hereafter, we set $\gamma = 5/3$. From the conservation equations of mass flux and momentum flux, the mass density and pressure in the region behind the end of the cooling layer are represented as a function of the velocity u'_2 ,

$$\begin{aligned} \rho_2 &= \frac{\rho_1 u'_1}{u'_2} = \frac{\gamma+1}{(\gamma-1)(1-\delta)}\rho_0, \\ p_2 &= (\rho_1 u'_1)(u'_1 - u'_2) + p_1 = \frac{2+(1-\gamma)\delta}{\gamma+1}\rho_0 V_{sh}^2, \end{aligned} \quad (22)$$

where $\delta = 1 - u'_2/u'_1$. Let the energy flux be

$$F = u\left(\frac{\rho u^2}{2} + h\right),$$

where h is the enthalpy per unit volume. We find that the fraction of energy flux lost via cooling is

$$\varepsilon = 1 - \frac{F(u'_2)}{F(u'_1)} = \frac{\delta}{1+\gamma} [2 + (\gamma-1)\delta]. \quad (23)$$

Following Liang & Keilby (2000), we parameterize the down-

stream velocity measured in the shock frame u'_2 as

$$u'_2 = \frac{\gamma_1 - 1}{\gamma_1 + 1} V_{sh}.$$

Then, we obtain

$$\delta = 1 - \frac{u'_2}{u'_1} = 1 - \frac{\gamma+1}{\gamma-1} \frac{\gamma_1-1}{\gamma_1+1}, \quad (24)$$

$$\rho_2 = \frac{\gamma_1+1}{\gamma_1-1}\rho_0, \quad (25)$$

$$p_2 = \frac{2}{\gamma_1+1}\rho_0 V_{sh}^2, \quad (26)$$

$$\varepsilon = \frac{4(\gamma-\gamma_1)}{(\gamma_1+1)^2(\gamma-1)}. \quad (27)$$

Note that γ_1 is *not* an adiabatic index although it gives the effective compression ratio as

$$R_c = \frac{\rho_2}{\rho_0} = \frac{\gamma_1+1}{\gamma_1-1}. \quad (28)$$

Following Ghavamian et al. (2002) and Heng & McCray (2007), we assume the downstream temperature of protons (T_p) and electrons (T_e) are related to the shock velocity, V_{sh} , and given by

$$\begin{aligned} kT_p &= (1-\eta) \frac{2(\gamma-1)}{(\gamma+1)^2} (\mu_\odot f_{eq} + 1 - f_{eq}) m_p V_{sh}^2, \\ &\equiv (1-\eta) \frac{2(\gamma-1)}{(\gamma+1)^2} \mu m_p V_{sh}^2, \\ kT_e &= (1-\eta) \frac{2(\gamma-1)}{(\gamma+1)^2} \left\{ \mu_\odot f_{eq} + \frac{m_e}{m_p} (1 - f_{eq}) \right\} m_p V_{sh}^2 \\ &\equiv \beta kT_p \end{aligned} \quad (29)$$

respectively. The definition of the energy loss rate η is the same as Eq. (1). We additionally define the temperature ratio $\beta = T_e/T_p$. The $\mu_\odot = 0.62$ is the mean molecular weight for solar abundances. The situation $f_{eq} = 1$ ($f_{eq} = 0$) represents temperature equilibration (non-equilibration) among all the particles in the fluid. Here we consider the case in which α particles are in the temperature equilibrium. Thus, for $f_{eq} = 1$, the mean molecular weight coincides with the value for solar abundances. The effective mean molecular weight, $\mu \equiv \mu_\odot f_{eq} + 1 - f_{eq}$, is rewritten as a function of β ,

$$\mu = 1 - (1 - \mu_\odot) \frac{\beta - \frac{m_e}{m_p}}{\mu_\odot + (1 - \mu_\odot)\beta - \frac{m_e}{m_p}}. \quad (31)$$

Equations (25) and (26) also give the downstream proton temperature as

$$kT_p = \mu m_p \frac{p_2}{\rho_2} = \frac{2(\gamma_1-1)}{(\gamma_1+1)^2} \mu m_p V_{sh}^2, \quad (32)$$

so that we obtain a quadratic equation for γ_1 ,

$$\eta = 1 - \frac{(\gamma+1)^2}{\gamma-1} \frac{\gamma_1-1}{(\gamma_1+1)^2}. \quad (33)$$

We solve Eq. (33) as

$$\begin{aligned} \gamma_1 &= \frac{1}{1-\eta} \left[\left\{ \frac{1}{2} \frac{(\gamma+1)^2}{\gamma-1} - 1 + \eta \right\} \right. \\ &\quad \left. - \sqrt{\left\{ \frac{1}{2} \frac{(\gamma+1)^2}{\gamma-1} - 1 + \eta \right\}^2 - (1-\eta) \left\{ \frac{(\gamma+1)^2}{\gamma-1} + 1 - \eta \right\}} \right]. \end{aligned} \quad (34)$$

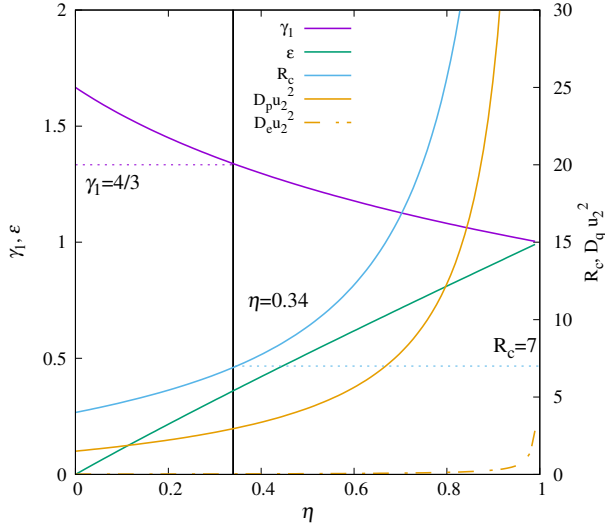


Figure 5. The relationships between η and γ_1 , ε , R_c and $D_q u_2^2 = m_q u_2^2 / (2kT_q)$. The left hand side vertical axis represents γ_1 and ε , and the right hand side shows R_c and $D_q u_2^2$. The purple line is γ_1 . The green line represents the energy loss fraction ε . The effective compression ratio R_c is shown by the light blue line. The orange solid line is $D_p u_2^2$ and the orange broken line is $D_e u_2^2$ for $\beta = 0.05$. The vertical black line in the panel is $\eta = 0.34$, where $\gamma_1 = 4/3$ and $R_c = 7$.

We take the minus sign in front of the square root in Eq. (34) to derive the physical solution satisfying $\gamma_1 = \gamma$ for $\eta = 0$. Hence, the compression ratio R_c is given by the energy loss rate η . The downstream velocity in the region behind the cooling layer u_2 , which is measured in the upstream frame, is derived from Eqs. (28) and (29) as

$$u_2 = \left(1 - \frac{1}{R_c}\right) V_{\text{sh}} = \left(1 - \frac{1}{R_c}\right) \sqrt{\frac{(\gamma + 1)^2}{2(\gamma - 1)} \frac{kT_p}{(1 - \eta)\mu m_p}}. \quad (35)$$

Figure 5 shows γ_1 , ε , R_c and $D_q u_2^2 = m_q u_2^2 / (2kT_q)$ as function of η . The representative value of $\eta = 0.34$ is illustrated by the vertical black line, where $\gamma_1 = 4/3$ and $R_c = 7$. We predict that highly polarized Balmer line emissions come from large $D_q u_2^2$. From the above formulae, setting the parameters T_p , η and β , we calculate the polarization degree from Eqs. (19) and (20). Note that for given downstream proton temperature T_p , a large energy loss rate η corresponds to a large shock velocity V_{sh} .

For typical young SNR, the temperature ratio, β , is estimated by the intensity ratio of the broad component of H α to narrow one, and to be $\beta \sim 0.03$ -0.07 (e.g. van Adelsberg et al. 2008). Furthermore, Laming (1990) showed that the polarized intensity depends on the proton temperature rather than the electron temperature. This fact arises from the stronger anisotropy of the proton's velocity distribution than that for the electrons, $D_e u_2^2 / (D_p u_2^2) = m_e / (m_p \beta) \ll 1$. Hence, the polarization intensity, Q_n , is mainly determined by the proton impacts. Indeed, the anisotropy of electron velocity distribution is very small as

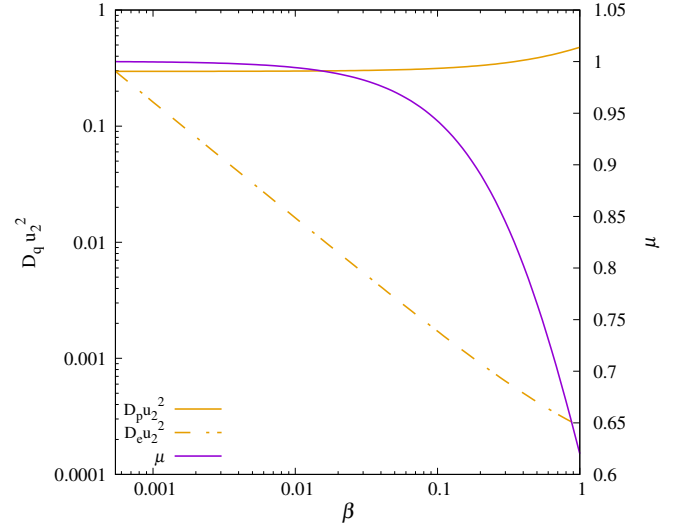


Figure 6. The anisotropy of velocity distribution of protons and electrons, $D_q u_2^2 = m_q u_2^2 / (2kT_q)$, and the effective mean molecular weight μ as function of β for $\eta = 0$. The left hand side vertical axis represents $D_q u_2^2$. The orange solid line is $D_p u_2^2$ and the orange broken line is $D_e u_2^2$. The purple line shows μ , whose value is represented by the right hand side vertical axis.

$D_e u_2^2 \approx m_e / (m_p \beta (1 - \eta)) \ll 1$. Since the electrons colliding with energy $E_e \gtrsim 10$ eV (equivalently $v_e \approx 2500$ km/s) excite the hydrogen atom, it contributes to Q_n in the case of $u_2 \gtrsim 2500$ km/s and $\beta \approx m_e / m_p$. However, the electron impacts yield unpolarized emission, that is, the polarization degree Q_n / I_n depends on the electron temperature. Figure 6 shows $D_q u_2^2$ and μ as function of β for $\eta = 0$.

3 THE POLARIZATION DEGREE OF H α EMISSION

In this section, we show the results of the observed polarization degree of H α emission.

First of all, we show the results for $\chi = \pi/2$ and $\beta = 0.05$. Figure 7 represents the observed polarization degree as a function of the energy loss rate η for Case A with fixed T_p . The solid lines show the results for $T_p = 0.47$ -16.9 keV (corresponding points are shown in the panel). For large η , the anisotropy of the proton velocity distribution becomes large (as shown in Fig. 5), resulting in larger polarization degree. For fixed T_p , large η yields large downstream velocity u_2 (see Eq. (35)). It means that the peak of the particle velocity distribution slides to the high velocity side but its width is fixed. When the downstream velocity u_2 is larger than ≈ 2500 km s $^{-1}$, the excitation rate of the hydrogen atoms by the electron impact becomes large, because almost all the electrons can excite the hydrogen atoms. That causes the large unpolarized intensity I_n and the small polarization degree Q_n / I_n .

Figure 8 represents the temperature dependence of the

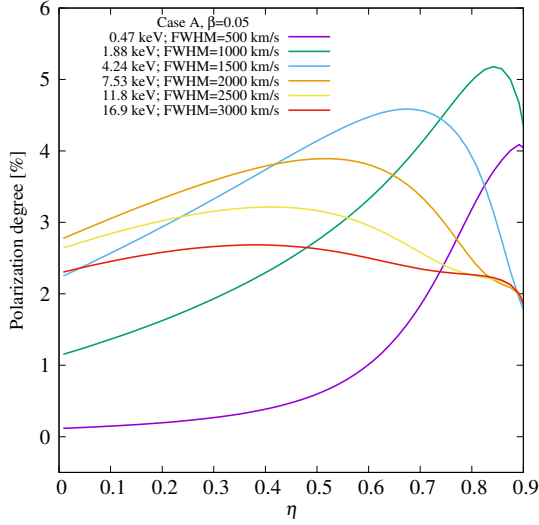


Figure 7. The polarization degree of H α as a function of η for fixed values of T_p (0.47, 1.88, 4.24, 7.53, and 16.9 keV) with given $\beta = 0.05$ and $\chi = \pi/2$ for Case A.

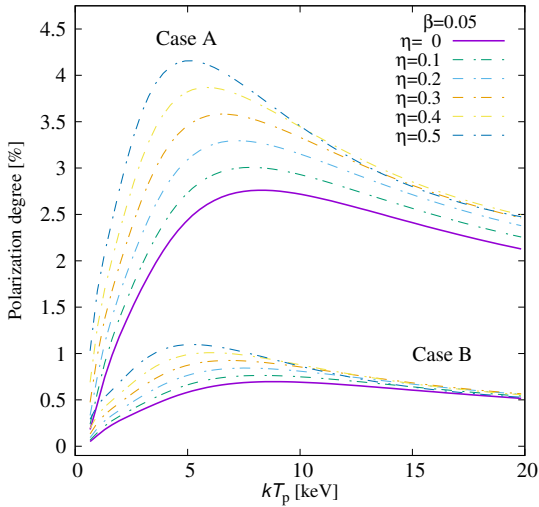


Figure 8. The polarization degree of H α as a function of T_p for fixed values of η (0, 0.1, 0.2, 0.3, 0.4, and 0.5) with given $\beta = 0.05$ and $\chi = \pi/2$ for Case A and Case B. The magenta lines show the result for $\eta = 0$ and the dashed lines are the results for $\eta = 0.1-0.5$ from bottom to top.

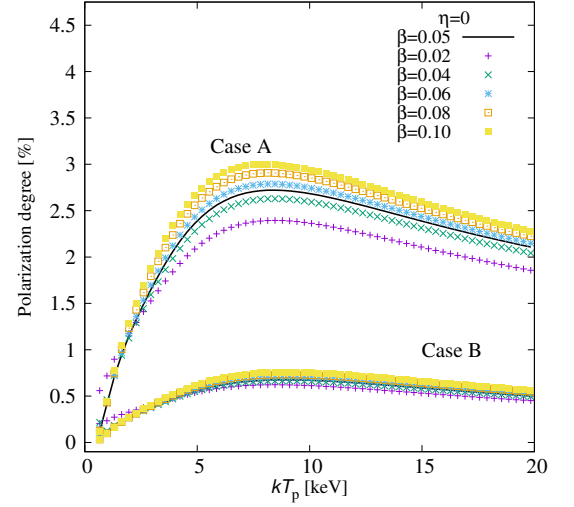


Figure 9. The polarization degree of H α as a function of T_p for fixed values of β (0.02, 0.04, 0.05, 0.06, 0.08 and 0.10) with given $\eta = 0.05$ and $\chi = \pi/2$ for Case A and Case B. The black lines show the result for $\beta = 0.05$ and the dashed lines are the results for $\beta = 0.02-0.1$ from bottom to top.

observed polarization degree for Cases A and B. The solid lines show the results of $\eta = 0$ and the dashed lines represent $\eta = 0.1-0.5$ from bottom to top. In Case B, the observed polarization degree is reduced due to the Lyman line trapping, yielding larger I_n . As shown in Figures 7 and 8, the significant energy loss rate is realized when the observed polarization degree is $\sim 4-5$ per cent (~ 1 per cent) for Case A (Case B).

We discuss the dependence of the polarization degree on β and χ . Figure 9 represents the observed polarization degree for Cases A and B for various fixed β . The solid lines correspond to the representative value of $\beta = 0.05$. The results of $\beta = 0.02-0.1$ are shown with points from bottom to top. For $T_p \gtrsim 5$ keV ($u_2/1600$ km/s)², a large fraction of electrons have an energy $E_e \gtrsim 10$ eV. Therefore, the β dependence is relatively large especially for Case A. On the other hand, for Case B, the effective cross section on electron impact $\sigma_{3p,e}$ is dominant (see the green and black curves in Figure 3). Since the excitation rate is proportional to $v_e \sigma_{3p,e}$, which is almost constant, the electron temperature dependence becomes weak.

The dependence on the viewing angle is shown in Figure 10. The points show $T_p = 0.47-16.9$ keV from bottom to top. The solid lines are $(Q_n/I_n)|_{\chi=\pi/2} \propto \sin^2 \chi$. The unpolarized intensity I_n is mainly determined by the electron impact due to the faster electron velocity than proton one. Since the velocity distribution of electron is nearly isotropic, the unpolarized intensity does not depend on the viewing angle. Thus, the polarization degree follows $Q_n/I_n \propto \sin^2 \chi$ (see Eq. (19)).

Figure 11 shows the total intensity ratio, $I_n(H\beta)/I_n(H\alpha)$ as a function of T_p for $\chi = \pi/2$ and $\beta = 0.05$ with

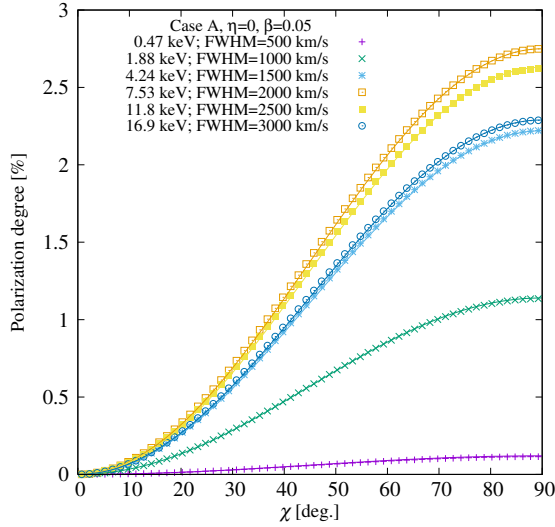


Figure 10. The polarization degree of H α as a function of the viewing angle χ for fixed values of T_p (0.47, 1.88, 4.24, 7.53, and 16.9 keV) with given $\beta = 0.05$ and $\eta = 0$ for Case A. The solid lines are $(Q_n/I_n)|_{\chi=\pi/2} \sin^2 \chi$.

fixed η . The dashed lines represent $\eta = 0-0.5$ from bottom to top. In Case A, the ratio of total cross sections, $\sigma_{\text{tot,p}}|_{I_n(\text{H}\beta)}/\sigma_{\text{tot,p}}|_{I_n(\text{H}\alpha)}$, is an increasing function of temperature in the range $1000 \text{ km s}^{-1} \lesssim v_p \lesssim 2000 \text{ km s}^{-1}$ (equivalently, $2 \text{ keV} \lesssim kT_p \lesssim 7.5 \text{ keV}$). Therefore, the total intensity ratio is increasing with T_p . On the other hand, in Case B, $I_n(\text{H}\alpha)$ increases by a factor of ~ 1.5 because of $B_{3p,2s} = 1$ and $B_{4p,3s} \approx 1$ (see the green and black curves in Figures 3 and 4). Therefore, the value of $I_n(\text{H}\beta)/I_n(\text{H}\alpha)$ is suppressed. Moreover, the ratio of total cross sections, $\sigma_{\text{tot,p}}|_{I_n(\text{H}\beta)}/\sigma_{\text{tot,p}}|_{I_n(\text{H}\alpha)}$, is almost constant for $1000 \text{ km s}^{-1} \lesssim v_p \lesssim 2000 \text{ km s}^{-1}$. Thus, the intensity ratio is constant with T_p . Likewise, the ratio depends on the electron temperature (Figure 12).

4 THE RATIO OF BALMER POLARIZED INTENSITIES

The polarization degree Q_n/I_n of Balmer line emission depends on the effective branching ratio, $B_{nl,n'l'}$, which includes the effect of Lyman line trapping. On the other hand, the polarized intensity Q_n is determined by the intrinsic $B_{nl,n'l'}$, which only depends on the spontaneous transition rates. Therefore, the polarized intensity ratio of Balmer line emission is not affected by Lyman line trapping. Moreover, the dependence of the viewing angle is also weak (see Eq. (19)). In addition, the electron velocity distribution is usually isotropic in SNRs for $\beta \gtrsim 0.01$ (see Figure 6). Thus, the electron temperature does not affect Q_n . Hence, the polarized intensity ratio measurements could be better than the measurements of the polarization degree for the estimation of η .

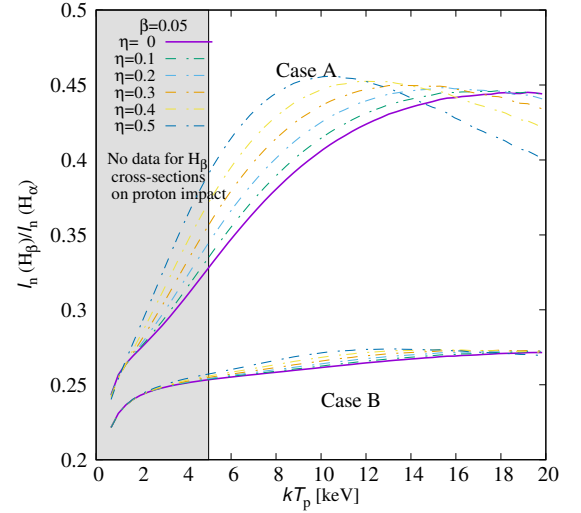


Figure 11. The total intensity ratio $I_n(\text{H}\beta)/I_n(\text{H}\alpha)$ as a function of T_p for fixed values of η (0, 0.1, 0.2, 0.3, 0.4, and 0.5) with given $\beta = 0.05$ and $\chi = \pi/2$ for Case A and Case B. The magenta lines show the result for $\eta = 0$ and the dashed lines are the results for $\eta = 0.1-0.5$ from bottom to top. The gray region indicates that the lack of cross section data for proton impact significantly affects the results, which are not reliable.

Figure 13 shows the polarized intensity ratio of H β to H α , $Q_n(\text{H}\beta)/Q_n(\text{H}\alpha)$, as a function of the energy loss rate η for $\beta = 0.05$ and $T_p = 0.47-16.9 \text{ keV}$ (corresponding points are shown in the panel). The T_p dependence of $Q_n(\text{H}\beta)/Q_n(\text{H}\alpha)$ is plotted in Figure 14. The lines show $\beta = 0.05$ and $\eta = 0-0.5$ from bottom to top. In particular, the ratio is increasing with η for $kT_p \lesssim 15 \text{ keV}$. The ratio of cross sections for proton impact of H β to H α , $\sigma_{\text{tot,p}}(\text{H}\beta)/\sigma_{\text{tot,p}}(\text{H}\alpha)$, is increasing with v_p for $v_p \lesssim 4000 \text{ km/s}$. Since higher loss rates η yield a larger number of high velocity protons with fixed T_p , the polarized intensity ratio is large. Figure 15 shows the ratio for different values of β , where all points with different colors are close to with each other. Thus, the polarized intensity ratio is not affected by β .

5 SUMMARY AND DISCUSSION

We have studied the linearly polarized Balmer line emission from the shocks that efficiently accelerate CRs. Our calculation has been generalized for arbitrary viewing angle. The Balmer line emission is polarized when collisions between the hydrogen atoms and the charged particles are anisotropic. In the downstream region of the shock with shock velocity V_{sh} , the charged particles (in particular protons) collide with the hydrogen atoms as a mildly-collimated beam in the rest frame of the hydrogen atoms. When a large fraction of SNR shock energy goes into CRs, the downstream temperature is lower than the adiabatic case without CR acceleration, resulting in a more anisotropic velocity distribution of charged

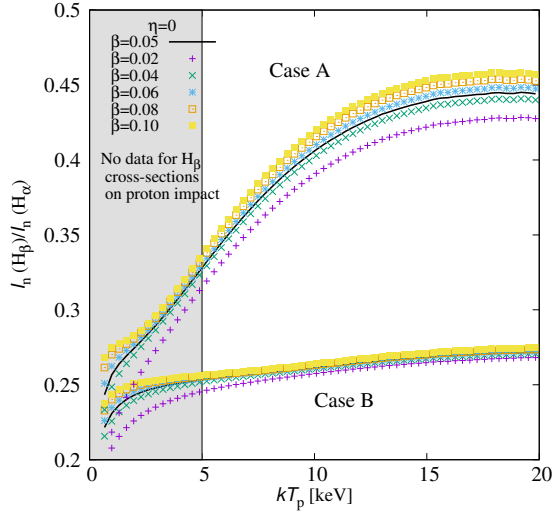


Figure 12. The total intensity ratio $I_n(\text{H}\beta)/I_n(\text{H}\alpha)$ as a function of T_p for fixed values of β (0.02, 0.04, 0.05, 0.06, 0.08, and 0.10) with given $\eta = 0.05$ and $\chi = \pi/2$ for Case A and Case B. The magenta lines show the result for $\beta = 0.05$ and the dashed lines are the results for $\beta = 0.02-0.1$ from bottom to top. The gray region indicates that the lack of cross section data for proton impact significantly affects the results, which are not reliable.

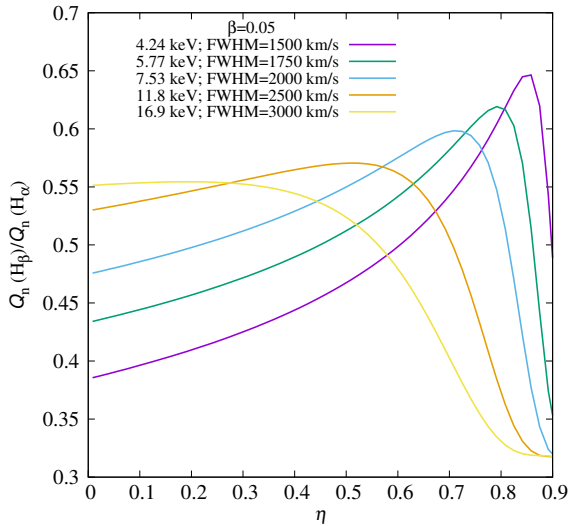


Figure 13. The polarized intensity ratio $Q_n(\text{H}\beta)/Q_n(\text{H}\alpha)$ as a function of η for fixed values of T_p ($= 4.24, 5.77, 7.53, 11.8,$ and 16.9 keV) with given $\beta = 0.05$.

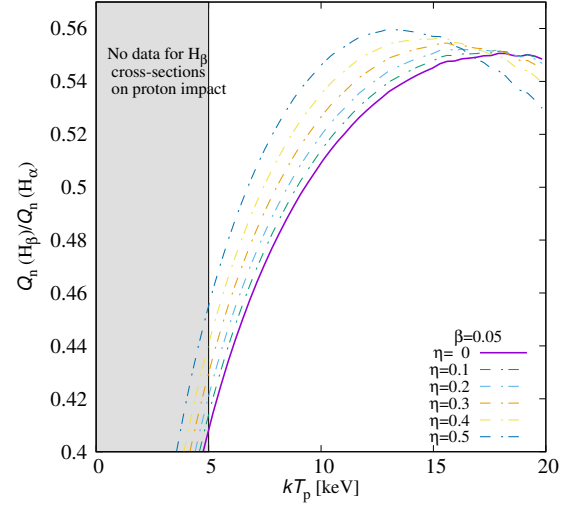


Figure 14. The polarized intensity ratio $Q_n(\text{H}\beta)/Q_n(\text{H}\alpha)$ as a function of T_p for fixed values of η (0, 0.1, 0.2, 0.3, 0.4, and 0.5) with given $\beta = 0.05$. The magenta lines show the result for $\eta = 0$ and the dashed lines are the results for $\eta = 0.1-0.5$ from bottom to top. The gray region indicates that the lack of cross section data for proton impact significantly affects the results, which are not reliable.

particles and higher polarization degree. In other words, for a given downstream temperature which is measured by the line width of the broad component of the $\text{H}\alpha$ emission, a large energy loss rate means a larger shock velocity than the prediction of Rankine-Hugoniot relations for adiabatic shocks, and consequently larger anisotropy of the velocity distribution. We have found that a higher energy loss rate η , which is defined in Eq. (29), yields higher polarized Balmer line intensity. In order to discriminate between Cases A or B in the optical depth of the Lyman lines, the total intensity ratio so-called Balmer decrement, $I_n(\text{H}\alpha)/I_n(\text{H}\beta)$, has been presented. Furthermore, we have shown that the energy loss rate η can be estimated by the polarized Balmer line intensity ratio $Q_n(\text{H}\beta)/Q_n(\text{H}\alpha)$ without uncertainties of the viewing angle, the electron temperature and the Lyman line trapping.

Since there are no cross section data on proton impact excitation to $n = 4$ in the range $v_p \lesssim 1000 \text{ km s}^{-1}$ (equivalently for downstream temperature less than ≈ 5 keV), our present results are applicable for young SNRs whose downstream temperature is typically observed as $T_p \gtrsim 5$ keV (for example T_p is 10 keV and 6–7 keV for SN 1006, Kepler and Tycho respectively: Fesen et al. 1989; Ghavamian et al. 2001, 2002). For older SNRs, T_p is smaller than 5 keV (e.g. $T_p \approx 0.1$ keV for Cygnus Loop: Medina et al. 2014). An exception can be seen for young SNR, RCW 86 possibly showing a high energy loss rate, has $T_p \approx 2$ keV (Helder et al. 2009). Therefore, to measure the energy loss rate in RCW 86 by the polarized Balmer-intensity ratio $Q_n(\text{H}\beta)/Q_n(\text{H}\alpha)$, additional atomic data are necessary.

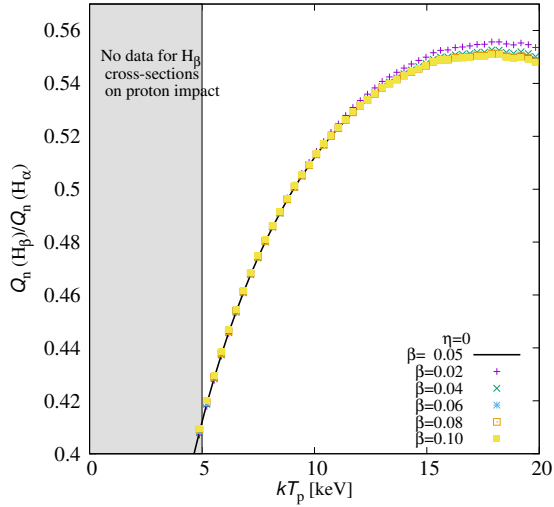


Figure 15. The polarized intensity ratio $Q_n(\text{H}\beta)/Q_n(\text{H}\alpha)$ as a function of T_p for fixed values of β (0.02, 0.04, 0.05, 0.06, 0.08, and 0.10) with given $\eta = 0$. The black line shows the result for $\beta = 0.05$ and the points are the results for $\beta = 0.02-0.1$, that overlap the black line. The gray region indicates that the lack of cross section data for proton impact significantly affects the results, which are not reliable.

Cargill & Papadopoulos (1988) pointed out that electrons may be heated at SNR shocks by plasma instabilities, such as Buneman and ion acoustic instabilities. This electron heating would be anisotropic, directed along the shock velocity, give rise to a different polarization signal in the Balmer lines. Electron heating by lower hybrid waves in a shock precursor (e.g. McClements et al. 1997; Laming et al. 2014) would be directed along the local magnetic field leading to a different polarization direction. However, the magnetic field can be highly disturbed by the CR-streaming instability at a gyroradius scale of CRs in the GeV energy, $r_g \sim 10^{13} \text{ cm}(E/1 \text{ GeV})(B/1 \mu\text{G})^{-1}$, (e.g. Bell 1978). Since the length scale of this disturbance is much smaller than the size of the emission region ($\sim 10^{16} \text{ cm}$), the magnetic field orientation becomes isotropic in the emission region. Thus on average, the highly disturbed field makes net direction of electron-hydrogen atom collision isotropic on our line of sight. As a result, the anisotropic heating of electrons directed along the magnetic field does not yield net polarization of the observed Balmer line emissions. Therefore, the present results can be valid when the magnetic field is highly disturbed at the scale smaller than the mean free path of the atomic collision. Besides, when the anisotropic electrons collide with other ionized species such as Mg, Si, S and Fe, the polarized X-ray line emissions from these species are detectable by future observation. We will study impacts of the anisotropic heating on Balmer line polarization in a separate paper.

For SN 1006 and Tycho’s SNR, we calculate the polarization degree, the total intensity ratio $I_n(\text{H}\beta)/I_n(\text{H}\alpha)$ and the

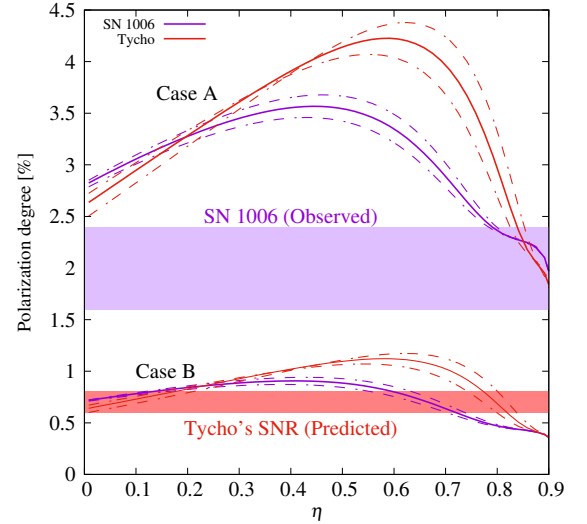


Figure 16. Polarization degree of $\text{H}\alpha$ as a function of η for SN 1006 (magenta) and Tycho’s SNR (red). The broken lines indicate uncertainties of the observed proton temperature. The horizontal magenta belt shows the range of observed polarization degree in SN 1006, $Q_n/I_n = 0.16-0.24$. The reddish bar illustrates predicted polarization degree in Case B for Tycho’s SNR ($\eta = 0.8$).

polarized intensity ratio $Q_n(\text{H}\beta)/Q_n(\text{H}\alpha)$. Figure 16 shows the polarization degree as a function of η . The total (polarized) intensity ratio is represented in Figure 17 (Figure 18). For SN 1006 (Tycho’s SNR), we set the proton temperature $kT_p = 9.87 \pm 0.68$ ($kT_p = 5.86 \pm 0.76$) and $\beta = 0.06$ ($\beta = 0.05$) following Ghavamian et al. (2001, 2002) and van Adelsberg et al. (2008). Here, the viewing angle is fixed at $\chi = \pi/2$.

Sparks et al. (2015) observed the polarized $\text{H}\alpha$ emission, whose polarization degree is $\approx 2.0 \pm 0.4$ per cent, and that of $\text{H}\beta$ simultaneously in north-west region of SN 1006. If we consider Case A for SN 1006, the observed polarization degree implies very high energy loss rate as $\eta \gtrsim 0.8$ (see Figure 16). In this case, the total intensity ratio $I_n(\text{H}\beta)/I_n(\text{H}\alpha)$ ranges between 0.3 and 0.35 (see Figure 17). On the other hand, in Case B, the predicted polarization degree is smaller than ~ 1 per cent. As shown in Figures 8 and 16, the polarization degree of $\text{H}\alpha$ emission is significantly affected by the optical depth of Ly β photon, $\tau(\text{Ly}\beta)$, which is evaluated from $I_n(\text{H}\beta)/I_n(\text{H}\alpha)$. Ghavamian et al. (2002) analyzed the spectra of Balmer line emissions at the same region as Sparks et al. (2015) did, and obtained $I_n(\text{H}\beta)/I_n(\text{H}\alpha) = 0.25-0.37$. Combining the model of Balmer line spectra, Ghavamian et al. (2002) concluded that $\tau(\text{Ly}\beta) \sim 0.5$. In our calculation for the optically thin and thick limits with $\eta = 0$, the ratio $I_n(\text{H}\beta)/I_n(\text{H}\alpha)$ ranges between 0.26 and 0.41, which is consistent with observational consequences that SN 1006 is in between Cases A and B without CR acceleration. Extending the present model to an arbitrary $\tau(\text{Ly}\beta)$, we will precisely estimate the energy loss rate η from the polarization degree of $\text{H}\alpha$ emissions, which will be studied in the sep-

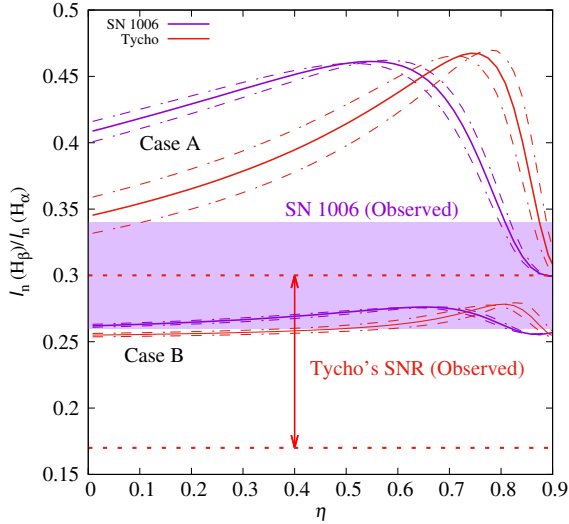


Figure 17. Total intensity ratio $I_n(\text{H}\beta)/I_n(\text{H}\alpha)$ for SN 1006 (magenta) and Tycho’s SNR (red). The broken lines indicate uncertainties of the observed proton temperature. The observed intensity ratio in SN 1006, $I_n(\text{H}\beta)/I_n(\text{H}\alpha) = 0.25\text{--}0.37$, is represented by horizontal magenta belt. The width between the two horizontal red dotted lines represents range of observed intensity ratio for Tycho’s SNR ($I_n(\text{H}\beta)/I_n(\text{H}\alpha) = 0.17\text{--}0.3$).

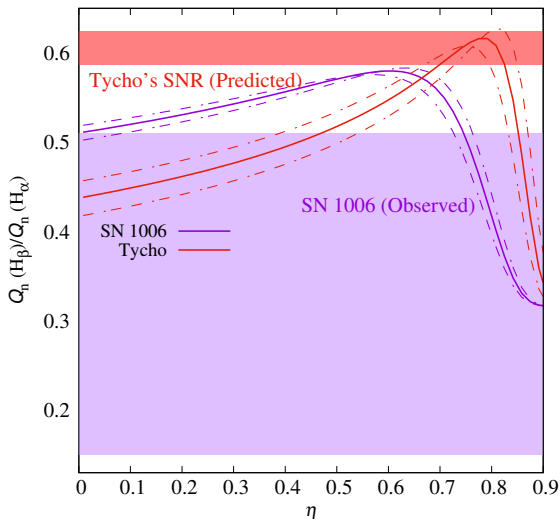


Figure 18. Polarized intensity ratio $Q_n(\text{H}\beta)/Q_n(\text{H}\alpha)$ for SN 1006 (magenta) and Tycho’s SNR (red). The broken lines indicate uncertainties of the observed proton temperature. The reddish bar indicates predicted intensity ratio for Tycho’s SNR ($\eta = 0.8$).

arate paper. Note that the energy loss rate η is also related to the ratio $Q_n(\text{H}\beta)/Q_n(\text{H}\alpha)$ and independent of $\tau(\text{Ly}\beta)$. For $\eta \gtrsim 0.8$, we predict that the polarized intensity ratio has $Q_n(\text{H}\beta)/Q_n(\text{H}\alpha) = 0.31\text{--}0.42$ (see Figure 18), whereas the observed value is poorly constrained, $Q_n(\text{H}\beta)/Q_n(\text{H}\alpha) \approx 0.33 \pm 0.18$, because the emission is too faint.

The eastern region of Tycho’s SNR has $\text{H}\alpha$ emissions, that is known as “knot g ” (Kamper & Bergh 1978). The proper motion of “knot g ” was measured as ≈ 0.2 arcsec yr^{-1} (Kamper & Bergh 1978). On the other hand, Hayato et al. (2010) observed the expansion velocity, ≈ 4700 km s^{-1} , from the Doppler shift of Si X-ray line. Combining the proper motion of the Si-rich layer (≈ 0.25 arcsec yr^{-1}) measured by Katsuda et al. (2010), they concluded that the distance of Tycho’s SNR is $\approx 4.0 \pm 1.0$ kpc. Thus, we expect the shock velocity of the “knot g ” region to be $V_{\text{sh}} \approx 4000$ km/s. The predicted temperature from Rankine-Hugoniot relation, $T_{\text{RH}} \approx 31$ keV, is much higher than the observed downstream temperature, $T_{\text{down}} \approx 6$ keV. Combining these measurements, the energy loss rate is estimated as $\eta \approx 0.8$ from Eq. (1). Furthermore, Warren et al. (2005) showed that the ratio of the forward shock radius to that of the contact discontinuity is $1 : 0.93$, which implies significant energy loss around the forward shock. This argument is independent of the uncertain distance. However, the eastern region of Tycho’s SNR (“knot g ”) was not considered in their analysis. Ghavamian et al. (2001) measured the intensity ratio $I_n(\text{H}\beta)/I_n(\text{H}\alpha)$ to be $0.087\text{--}0.115$ (unreddened), which becomes $0.17\text{--}0.3$ after correcting for the visual extinction of $1.6 \leq A_v \leq 3.2$, where we take the lower and the upper limits from optical (Chevalier, Kirshner & Raymond 1980) and X-ray absorption measurements (Cassam-Chenaï et al. 2007), respectively. Observational results, $\eta = 0.8$ and $I_n(\text{H}\beta)/I_n(\text{H}\alpha) = 0.17\text{--}0.3$, prefer Case B. Then, $Q_n/I_n \approx 0.6\text{--}0.8$ per cent is expected. Note that the energy loss rate inferred from the polarization measurements does not depend on the distance of SNR.

The polarization degree depends on the electron temperature, the optical depth and the viewing angle of the shock. These unknowns cause uncertainty of the observed polarization degree, although the optical depth of the Lyman line emissions and the electron temperature can be measured by observations of $I_n(\text{H}\alpha)/I_n(\text{H}\beta)$ and the ratio of the intensity of broad component of $\text{H}\alpha$ emission to that of narrow component, $I_b(\text{H}\alpha)/I_n(\text{H}\alpha)$. A large energy loss rate measured by the polarization degree of $\text{H}\alpha$ emissions can be confirmed by the polarized intensity ratio, $Q_n(\text{H}\beta)/Q_n(\text{H}\alpha)$, which does not depend on the above values. As the energy loss rate is expected to be $\eta \approx 0.8$ in Tycho’s SNR, we predict $Q_n(\text{H}\beta)/Q_n(\text{H}\alpha) \approx 0.60$ (see Figure 18).

Shimoda et al. (2015) pointed out that the density fluctuations in realistic ISM make the SNR shock rippled and oblique everywhere. In such a situation, the kinetic energy flux in the direction perpendicular to the shock normal is not completely dissipated, which causes lower downstream temperature compared with the uniform, ideal ISM case and yields apparent energy loss. The non-dissipating kinetic energy goes to the downstream fluid motions with the apparent energy loss rate is estimated as $\eta \approx (\Delta\rho/\langle\rho\rangle_0)^2$ (see Appendix in Shimoda et al. 2015), where $\Delta\rho/\langle\rho\rangle_0$ is the amplitude of the density fluctuation and its value is typically $\Delta\rho/\langle\rho\rangle_0 \sim 0.3$ (e.g. Inoue et al. 2013). Therefore, the impacts

of the energy loss owing to the shock rippling is modest for the polarization degree of Balmer line emissions. The polarized Balmer emissions from a realistic SNR shock will be studied elsewhere.

We have assumed that the shock wave losing its energy owing to the CR acceleration does not affect its shock structure, and calculated the polarized Balmer line intensities from the downstream region. If the CRs remain in the shock and CR pressure becomes comparable to the ram pressure in the far upstream region, then the charged particles are decelerated by the back reaction of CRs, leading to the modification of the shock structure in the upstream region adjacent to the shock surface (e.g. [Berezhko & Ellison 1999](#)). The decelerated charged particles colliding the hydrogen atoms in the upstream region are well-collimated in the rest frame of hydrogen atom (e.g. $D_p u_1^2 \sim 10^{2-3} (u_1/500 \text{ km s}^{-1})^2 (T_p/1-10 \text{ eV})^{-1} \gg 1$). The Balmer line emissions from such hydrogen atoms are also highly polarized. Therefore, detecting the polarized Balmer line emission from the upstream region becomes evidence for the modification of the shock structure. We will extend the present model to study the polarized Balmer line emissions from upstream region in forthcoming paper.

ACKNOWLEDGEMENTS

We thank Drs. Aiko Takamine and Shota Kisaka for valuable comments to complete this work. We also thank the referee, John Raymond, for his comments to further improve the paper. This work is supported by Grant-in-aids for JSPS Fellows (15J08894, JS) and JSPS KAKENHI Grants: 16K17702 (YO), 15K05088 (RY) and 16K17673 (SK), NASA grants NNM16AAA36I (Chandra GO) and NNG16FC61I (HST GO) and Basic research Funds of the CNR (JML).

REFERENCES

- Balança C., & N. Feautrier N., 1998, *A&A*, 334, 1136
 Barnett C. F., et al., 1990, NASA STI/Recon Technical Report N, 91, 13238
 Bell A. R., 1978, *MNRAS*, 182, 147
 Berezhko E. G., & Ellison D. C., 1999, *ApJ*, 526, 385
 Blasi P., Morlino G., Bandiera R., Amato E., & Caprioli D., 2012, *ApJ*, 755, 121
 Bray I., & Stelb A. T., 1995, *Calculation of electrons scattering on hydrogenic targets*, AAMP 35, 209
 Cargill, P. J., & Papadopoulos, K. 1988, *ApJ*, 329, L29
 Cassam-Chenaï G., et al. 2007, *ApJ*, 665, 315
 Chevalier R. A., Kirshner R. P., & Raymond J. C. 1980, *ApJ*, 235, 186
 Chevalier R. A., & Raymond J. C. 1978, *ApJ*, 225, L27
 Cohen E., Piran T., & Sari R., 1998, *ApJ*, 509, 717
 Fesen R. A., Becker R. H., Blair W. P., & Long K. S. 1989, *ApJ*, 338, L13
 Ghavamian P., Raymond J. C., Hartigan P., & Blair, W. P. 2000, *ApJ*, 535, 266
 Ghavamian P., Raymond J. C., Smith R. C., & Hartigan P. 2001, *ApJ*, 547, 995
 Ghavamian P., Winkler P. F., Raymond J. C., & Long K. S. 2002, *ApJ*, 572, 888
 Hayato A., et al., 2010, *ApJ*, 725, 894
 Helder, E. A., Vink, J., Bassa, C. G., et al. 2009, *Sci*, 325, 719
 Helder, E. A., Vink, J., Bamba, et al. 2013, *MNRAS*, 435, 910
 Heng, K., & McCray, R. 2007, *ApJ*, 654, 923
 Heng K., & Sunyaev R. A., 2008, *A&A*, 481, 117
 Heng K., 2010, *PASA*, 27, 23
 Hughes, J. P., Rakowski, C. E., & Decourchelle, A. 2000, *ApJL*, 543, L61
 Inoue T., Shimoda J., Ohira Y., & Yamazaki R. 2013, *ApJL*, 772, L20
 Janev R. K., & Smith J. J. 1993, *Cross Sections for Collision Processes of Hydrogen Atoms with Electrons, Protons and Multiply Charged Ions* (Vienna: IAEA)
 Jakimov D., & Janev R. K., 2015, *Phys. of Plasmas*, 22, 103301
 Kamper K., & van den Bergh S., 1978, *ApJ*, 224, 851
 Katsuda S., et al., 2010, *ApJ*, 709, 1387
 Katsuda S., et al., 2016, *ApJ*, 819, L32
 Kleinpoppen H., & Kraiss, E. 1968, *Phys. Rev. Lett.*, 20, 361
 Knežević S., et al., 2016, preprint (arXiv:1609.03356)
 Laming J. M., 1990, *ApJ*, 362, 219
 Laming J. M., et al. 2014, *ApJ*, 790, 11
 Lee J., Koo B., Raymond J. C., Ghavamian, P., Pyo T., Tajitsu A., & Hayashi M., 2007, *ApJ*, 659, L133
 Lee, J., et al. 2010, *ApJ*, 715, L146
 Lim, A. J., & Raga A. C., 1996, *MNRAS*, 280, 103
 Laing E., & Keilty K., 2000, *ApJ*, 533, 890
 McClements, K. G., et al., 1997, *MNRAS*, 291, 241
 McConkey J. W., 1988, *J. Phys.*, 21, L317
 Medina A. A., et al., 2014, *ApJ*, 791, 30
 Morlino G., Bandiera R., Blasi P., & Amato E. 2012, *ApJ*, 760, 137
 Morlino G., Blasi P., Bandiera R., & Amato E. 2013a, *A&A*, 557, A142
 Morlino G., Blasi P., Bandiera R., Amato E., & Caprioli D., 2013b, *ApJ*, 768, 148
 Morlino G., Blasi P., Bandiera R., & Amato E. 2014, *A&A*, 562, A141
 Ohira, Y., & Takahara, F. 2007, *ApJL*, 661, L171
 Ohira, Y., & Takahara, F. 2008, *ApJ*, 688, 320
 Ohira Y. 2012, *ApJ*, 758, 97
 Ohira, Y. 2013, *Phys. Rev. Lett.*, 111, 245002
 Ohira, Y. 2014, *MNRAS*, 440, 514
 Ohira, Y. 2016a, *ApJ*, 817, 137
 Ohira, Y. 2016b, *ApJ*, 827, 36
 Percival I. C., & Seaton M. J., 1958, *Philos. Trans. R. Soc. Lond.*, 251, 113
 Rakowski, C. E., Laming, J. M., & Ghavamian, P. 2008, *ApJ*, 684, 348
 Reynoso E. M., Hughes J. P., & Moffett D. A., 2013, *AJ*, 145, 104
 Shimoda J., Inoue T., Ohira Y., Yamazaki R., Bamba A., & Vink J., 2015, *ApJ*, 803, 98
 Sparks W. B., et al., 2014, *ApJ*, 780, 66
 Sparks W. B., Pringle J. E., Carswell R. F., et al. 2015, *ApJL*, 815, L9
 Syms R. F., McDowell M. R. C., Morgan L. A., Myerscough V. P., *J. Phys. B: Atomic, Molecular, and Opt. Phys.*, 8, 17, 2817
 Takács et al. 1996, *Phys. Rev. A*, 54, 2
 Tatischeff, V., & Hernanz, M. 2007, *ApJL*, 663, L101
 Tseliakhovich D., Hirata C. M., & Heng K., 2012, *MNRAS*, 422, 2357
 van Adelsberg M., Heng K., McCray R., & Raymond J. C., 2008, *ApJ*, 689, 1089
 Warren J. S., et al., 2005, *ApJ*, 634, 376

This paper has been typeset from a $\text{\TeX}/\text{\LaTeX}$ file prepared by the author.